

# Through-Space Aromatic Character in Excimers

Vishnu Vijay<sup>‡</sup>, Meera Madhu<sup>‡</sup>, Remya Ramakrishnan, Alfy Benny and Mahesh Hariharan\*

School of Chemistry, Indian Institute of Science Education and Research Thiruvananthapuram  
(IISER-TVM), Maruthamala P. O., Vithura, Thiruvananthapuram 695551, Kerala, India.

## Electronic Supplementary Information

### Contents

<b>Section A: Computational Techniques</b> .....	2
<b>Geometry Optimization</b> .....	2
<b>Nucleus Independent Chemical Shift (NICS)</b> .....	2
<b>Gauge Including Magnetic Induced Current (GIMIC)</b> .....	3
<b>Electron Localization Function (ELF)</b> .....	3
<b>Harmonic Oscillator Model of Aromaticity (HOMA)</b> .....	3
<b>Bond Length Alteration (BLA)</b> .....	3
<b>Section B: Tables</b> .....	4
<b>Section C: Figures</b> .....	6
<b>Section D: References</b> .....	10

## Section A: Computational Techniques

**Geometry Optimization:** The geometries of both monomers and excimers in T<sub>1</sub> were optimized at SOS-CIS(D<sub>0</sub>)/aug-cc-pVDZ level of theory from the ground state monomer geometries calculated at SOSMP2/aug-cc-pVDZ level. All the geometry optimizations were performed using the Q-Chem program package (version 5.2) with the IQmol molecule viewer as the user interface.<sup>1</sup> The multiconfigurational character of the systems were delineated using CASSCF calculations using 6-31G basis set. Previous studies have reported triplet monomers of benzene, naphthalene and anthracene to have a single dominating configuration.<sup>2</sup> In the case of benzene excimer, all the  $\pi$ -orbitals were considered as the active space (12, 12). For naphthalene and anthracene dimers, the active space consisted of eight highest filled  $\pi$ -orbitals (16, 16). The weights of the two most important configurations in the case of three excimers are given Table S1. The negligible weights of the second configuration demonstrate the single-configurational character of the excimers and thus DFT calculations are apt for these systems. For further calculations, SOS-CIS(D<sub>0</sub>)/aug-cc-pVDZ optimized structure are considered as this method takes into account dynamic correlations appropriately.<sup>3</sup> CASSCF calculations were carried out using Gaussian 16.<sup>4</sup>

**Nucleus Independent Chemical Shift (NICS):** NICS scan calculations were carried out using Gauge Including Atomic Orbital (GIAO) method at B3LYP/6-311+G\*\* level of theory<sup>5</sup> in Gaussian 09 software.<sup>6</sup> NICS-scan was performed for a series of ghost atoms placed at a separation of 0.1 Å along lines passing through the center of each ring, perpendicular to the molecular plane obtained using the AROMA software.<sup>7</sup> NICS values at CAM-B3LYP, LC- $\omega$ HPBE and M06-L with 6-311+G\*\* were done using Gaussian 16. The similar spin densities calculated for the constituent molecules of the excimers demonstrates the complete delocalization of the triplet biradical between the molecules even at long-range corrected functionals (Table S3-S5). The comparison of NICS(0) values of the triplet monomers and excimers exhibit reduction in antiaromaticity upon excimer formation, consistent with the other results. 2-D NICS plots were obtained using a grid of ghost atoms placed at a distance of 0.5 Å using B3LYP/6-311+G\*\* level of theory.

**Gauge Including Magnetic Induced Current (GIMIC):** The relationship between nuclear magnetic shielding tensor and the current density susceptibility tensor is given by Biot-Savart law. The GIMIC program calculates current density susceptibility tensor by a combination of Biot-Savart law and the analytic gradient expression for calculating NMR shielding tensors. The calculated current densities are gauge origin independent as the gauge including atomic orbitals (GIAOs) or London Atomic Orbitals (LAOs) are employed. The current density vector is visualized as streamline plots 1 Å above the molecular plane. The relative magnitude of the current vectors (represented by change in color code) indicate the dominating diatropic (clockwise) or paratropic (anticlockwise) contribution corresponding to aromatic or antiaromatic character. Integration of current density through bonds gives a quantitative measure of dominating current density flow.

The density matrices for GIMIC calculation was obtained via the nuclear magnetic shielding calculation done at B3LYP/6-311+G\*\* level of theory. The magnetically induced current densities were calculated using the GIMIC program.<sup>8-10</sup> The streamline plots are visualized using the line integral convolution (LIC) method as implemented in ParaView.<sup>11</sup>

**Electron Localization Function (ELF):** Aromaticity was probed based on the electron density of systems using ELF of Becke and Edgecombe.<sup>12</sup> The ELF, defined in terms of the excess of local kinetic energy density due to the Pauli Exclusion Principle and the Thomas-Fermi kinetic energy density, depicts the degree of electron delocalization. Higher values of ELF correspond to regions with higher probability to localize an electron. ELF<sub>π</sub> calculations involving the characteristics of π-electrons were carried out using Multiwfn package (version 3.6).<sup>13</sup> Input files (.wfn) were generated from the optimized molecules using the Q-Chem program package (version 5.2).

**Harmonic Oscillator Model of Aromaticity (HOMA):** HOMA values for all the rings in the molecules were calculated using Multiwfn package (version 3.6) with the formula:

$$\text{HOMA} = 1 - \frac{\alpha}{n} \sum_{i=1}^n (R_{opt} - R_i)^2$$

Where  $n$  is the number of C-C bonds in the ring and  $R_i$  corresponds to individual C-C bond lengths. The empirical constant,  $\alpha$  and the optimum value for C-C bond,  $R_{opt}$  were set to be 257.7 and 1.388 Å respectively. Although HOMA was originally developed for closed-shell systems, comparison of HOMA values depicting C-C bond length equalization can be correlated to aromaticity in T<sub>1</sub> as well.<sup>14</sup>

**Bond Length Alternation (BLA):** This index is expressed as the sum of the absolute values of the deviations of the particular bond lengths from the average bond lengths divided by the number of bonds.

$$\text{BLA} = \frac{1}{n} \sum_{i=1}^n (\bar{R}_i - R_i)$$

Where  $n$  is the number of C-C bonds in the ring and  $R_i$  corresponds to individual C-C bond lengths.<sup>15</sup>

## Section B: Tables

**Table S1.** Weights for the two most important configurations for the optimized geometries of the excimers.

	Weight of 1 <sup>st</sup> configuration	Weight of 2 <sup>nd</sup> configuration
Benzene excimer	0.67	0.06
Naphthalene excimer	0.99	0.00
Anthracene excimer	0.77	0.03

**Table S2.** Bond Length Alternations (BLAs) of the triplet excimers and the corresponding monomers.

		Bond Length Alteration values (Å)
<b>Benzene</b>	Monomer	0.058
	Excimer	0.028
<b>Naphthalene</b>	Monomer	0.030
	Excimer	0.012
<b>Anthracene</b>	Monomer	0.021
	Excimer	0.011

**Table S3.** Spin Densities and NICS values calculated at different functionals using 6-311G\*\* for benzene triplet monomer and excimer. Spin densities for the constituent molecules of the excimer are represented separated by forward-slash. NICS values are in units of ppm.

Functionals	NICS <sub>iso</sub> (0)		NICS <sub>zz</sub> (0)		NICS <sub>isocage</sub>	Spin Densities
	Excimer	Monomer	Excimer	Monomer		
B3LYP	19.71	29.01	83.44	97.38	11.93	0.99/1.00
CAM-B3LYP	17.13	32.66	76.23	108.64	7.76	0.99/1.02
LC- $\omega$ HPBE ( $\omega=0.10$ )	23.78	36.70	93.62	121.37	15.58	1.00/1.00
LC- $\omega$ HPBE ( $\omega=0.20$ )	19.93	34.06	83.33	110.30	11.13	0.98/ 1.02
M06-L	19.02	32.86	80.24	112.14	10.85	0.98/1.01

**Table S4.** Spin Densities and NICS values calculated at different functionals using 6-311G\*\* for naphthalene triplet monomer and excimer. Spin densities for the constituent molecules of the excimer are represented separated by forward-slash. NICS values are in units of ppm.

Functionals	NICS <sub>iso</sub> (0)		NICS <sub>zz</sub> (0)		NICS <sub>isocage</sub>	Spin Densities
	Excimer	Monomer	Excimer	Monomer		
B3LYP	5.03	12.64	35.42	50.79	-2.41	1.00/1.00
CAM-B3LYP	3.31	15.12	31.09	58.32	-4.65	1.00/1.02
LC- $\omega$ HPBE ( $\omega=0.10$ )	6.06	16.44	38.29	63.15	-1.41	1.00/1.00
LC- $\omega$ HPBE ( $\omega=0.20$ )	4.34	14.16	34.34	56.40	-3.49	1.00/1.00
M06-L	4.91	14.39	34.86	57.55	-1.98	1.00/1.00

**Table S5.** Spin Densities and NICS values calculated at different functionals using 6-311G\*\* for anthracene triplet monomer and excimer. Spin densities for the constituent molecules of the excimer are represented separated by forward-slash. NICS values are in units of ppm. C and T correspond to central and terminal rings respectively.

Functionals	NICS <sub>iso</sub> (0)				NICS <sub>zz</sub> (0)				NICS <sub>isocage</sub>	Spin Densities		
	Excimer		Monomer		Excimer		Monomer					
	C	T	C	T	C	T	C	T				
B3LYP	-0.77	-3.79	11.86	0.41	20.83	4.61	50.87	14.59	-9.55	-9.46 1.00/0.99		
CAM-B3LYP	-1.53	-5.19	13.29	2.71	20.12	1.04	55.16	21.52	9.58	-11.09 1.01/0.99		
LC- $\omega$ HPBE ( $\omega=0.10$ )	-0.49	-3.96	12.69	3.51	22.60	3.96	54.55	24.67	-7.06	-9.02 0.99/1.00		
LC- $\omega$ HPBE ( $\omega=0.20$ )	-0.34	-4.90	12.35	1.09	19.43	1.79	53.59	17.80	-8.58	-10.53 1.02/ 0.98		
M06-L	-1.02	-4.11	11.50	3.19	20.12	3.95	50.89	24.32	-6.85	-8.79 0.99/1.00		

## Section C: Figures

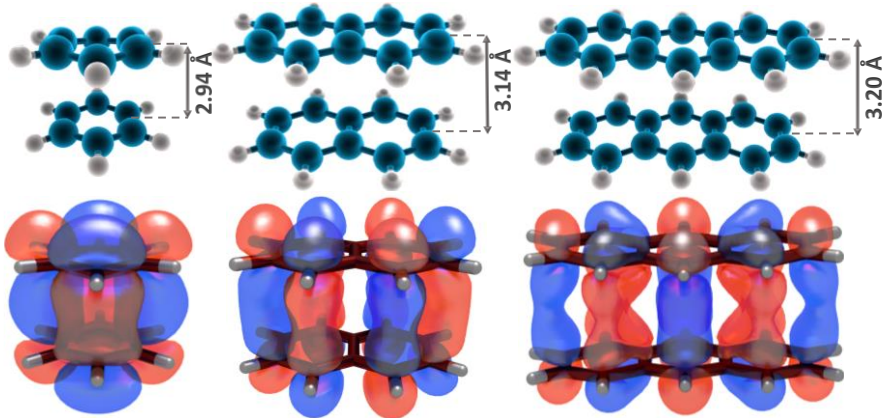


**Figure S1.** Structures of benzene, naphthalene and anthracene triplet excimers with the corresponding highest occupied molecular orbitals (isovalue = 0.02).

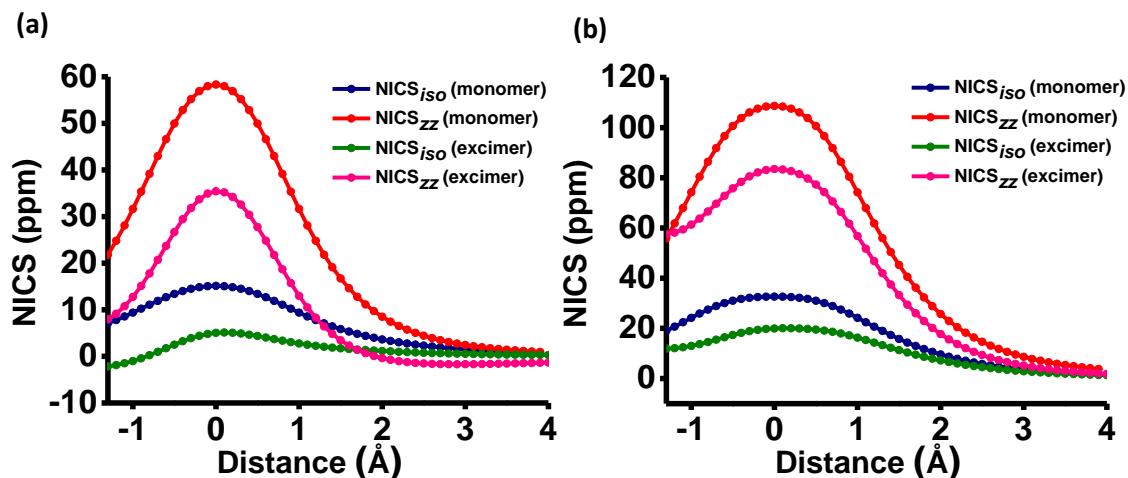


**Figure S2.** NICS scan values of  $T_1$  monomers and excimers in (a) benzene and (b) naphthalene at B3LYP/6-311+G\*\* level of theory.

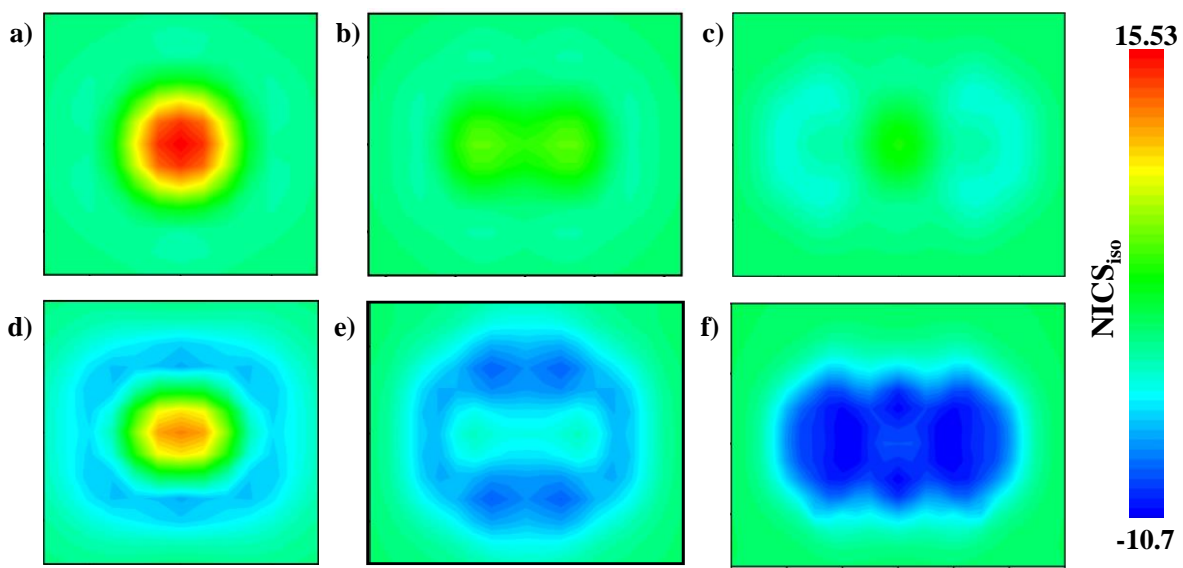


**Figure S3.** 2-D  $\text{NICS}_{iso}$  plots of a) benzene monomer, b) naphthalene monomer c) anthracene monomer d) benzene excimer, e) naphthalene excimer and f) anthracene excimer at B3LYP/6-311+G\*\* level of theory. The scale is in units of ppm.

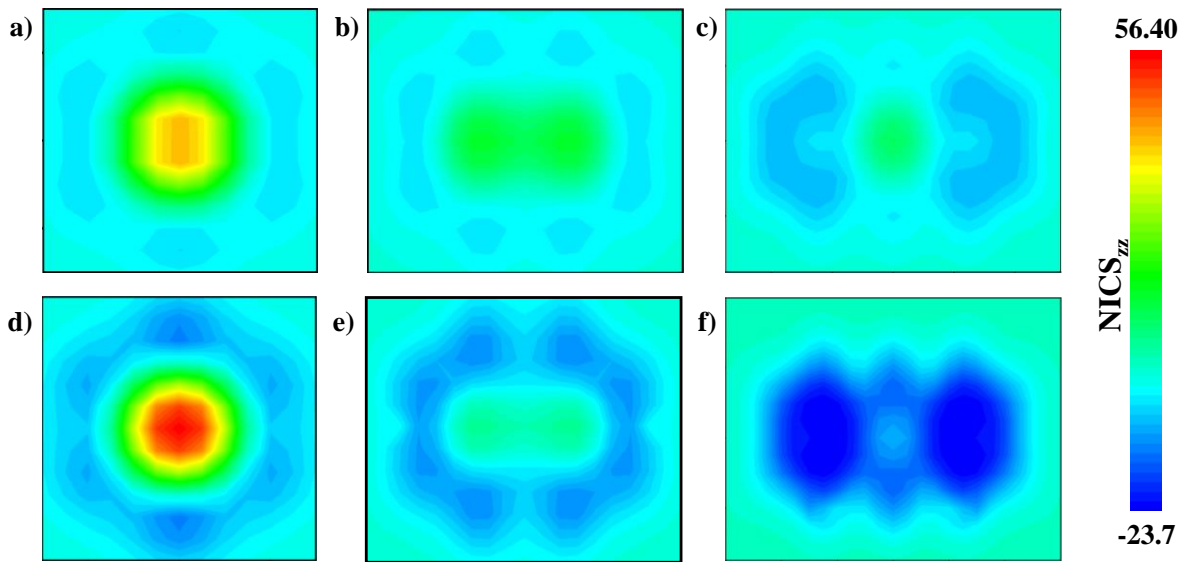


**Figure S4.** 2-D  $\text{NICS}_{zz}$  plots of a) benzene monomer, b) naphthalene monomer c) anthracene monomer d) benzene excimer, e) naphthalene excimer and f) anthracene excimer at B3LYP/6-311+G\*\* level of theory. The scale is in units of ppm.

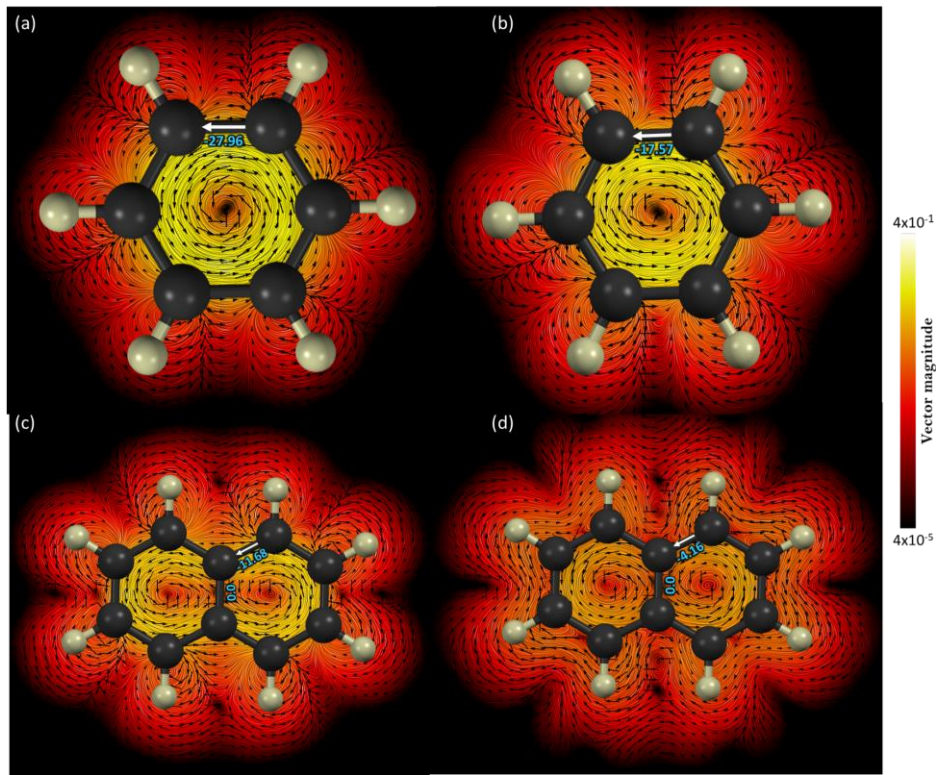


**Figure S5.** Current density vector field represented using line integral convolution (LIC) method for (a) benzene monomer (b) benzene excimer (c) naphthalene monomer and (d) naphthalene excimer, 1 Å above the molecular plane. Direction of local induced current vectors and the total current are shown as black and white arrows respectively with the total current strengths labeled in nA/T. Magnetic field is oriented towards the viewer.

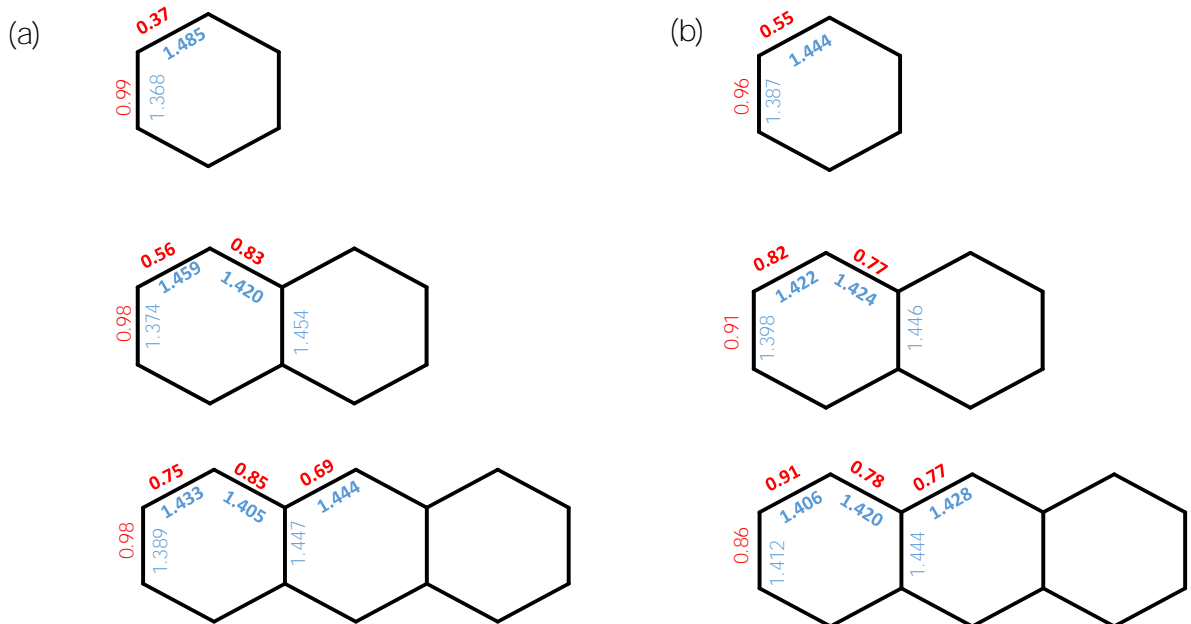


**Figure S6.** Bond lengths in Å (given in blue) and ELF<sub>π</sub> bifurcation values (given in red) for individual C-C bonds in  $T_1$  (a) monomers and (b) excimers.

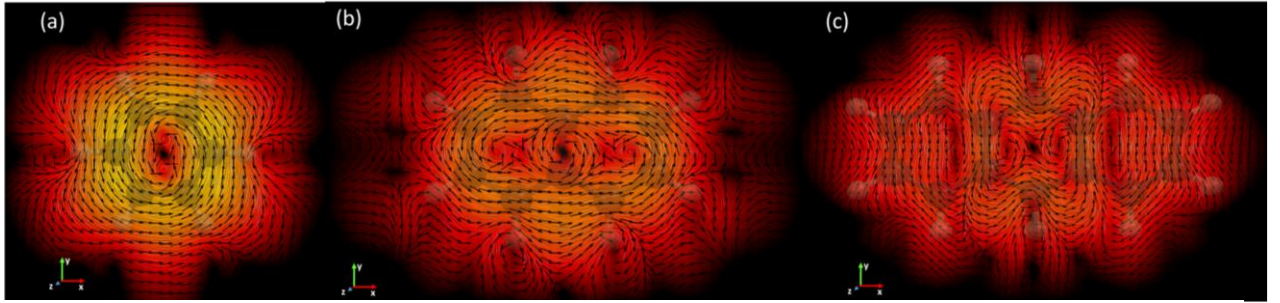


**Figure S7.** LIC plots of current density vector fields on the plane parallel to the molecular plane ( $XY$  plane) passing through the geometric center for (a) benzene (b) naphthalene and (c) anthracene excimers. Magnetic field is oriented in positive  $Z$  direction. Scale of the vector magnitude is same as in Fig. S3 for all LIC plots. Figure 3a in the manuscript has been reproduced as (c) for the sake of comparison.

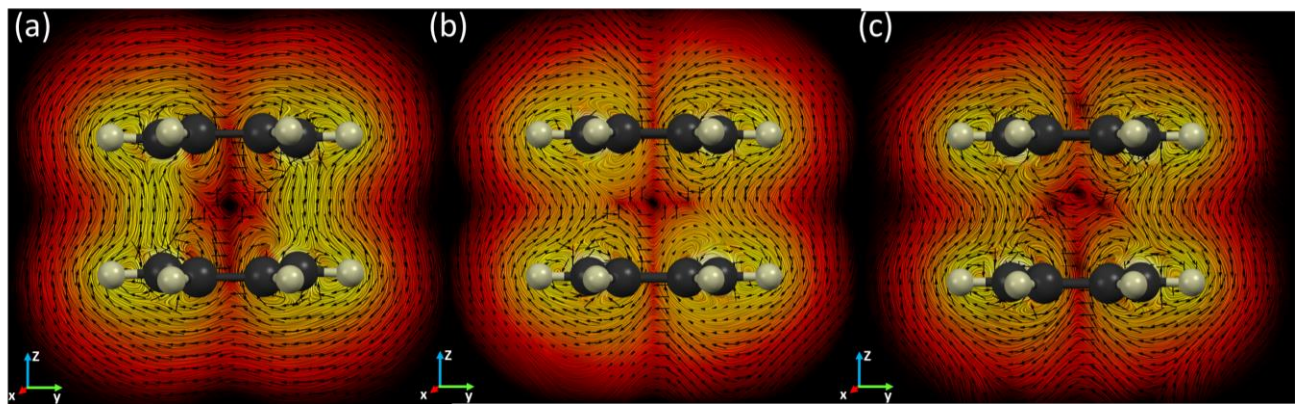


**Figure S8.** LIC plots of current density vector fields on the  $YZ$  plane passing through the centroids of the rings in (a) benzene (b) naphthalene and (c) anthracene excimers. Magnetic field is oriented in positive  $X$  direction. Figure 3b in the manuscript has been reproduced as (c) for the sake of comparison.

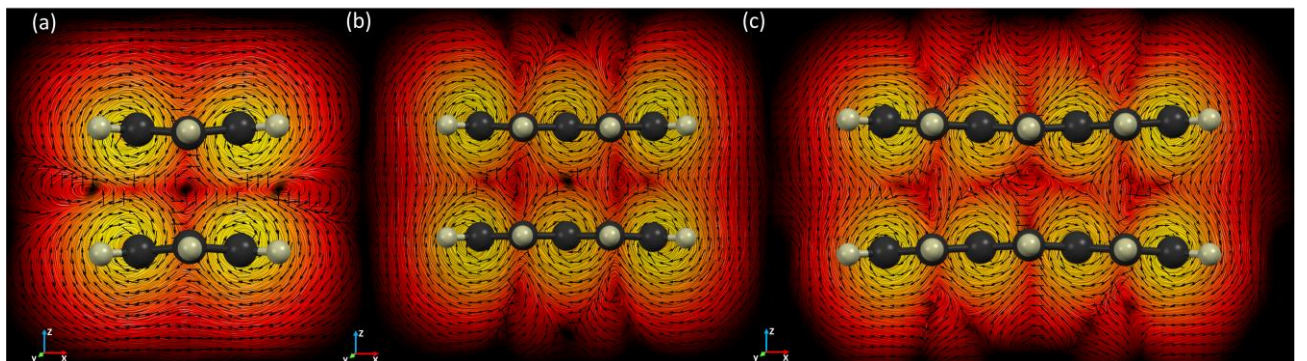


**Figure S9.** LIC plots of current density vector fields on the  $XZ$  plane passing through the geometric center for (a) benzene (b) naphthalene and (c) anthracene excimers. Magnetic field is oriented in positive  $Y$  direction.

## Section D: References

1. Y. Shao, Z. Gan, E. Epifanovsky, A. T. B. Gilbert, M. Wormit, J. Kussmann, A. W. Lange, A. Behn, J. Deng, X. Feng, D. Ghosh, M. Goldey, P. R. Horn, L. D. Jacobson, I. Kaliman, R. Z. Khaliullin, T. Kuś, A. Landau, J. Liu, E. I. Proynov, Y. M. Rhee, R. M. Richard, M. A. Rohrdanz, R. P. Steele, E. J. Sundstrom, H. L. Woodcock, P. M. Zimmerman, D. Zuev, B. Albrecht, E. Alguire, B. Austin, G. J. O. Beran, Y. A. Bernard, E. Berquist, K. Brandhorst, K. B. Bravaya, S. T. Brown, D. Casanova, C.-M. Chang, Y. Chen, S. H. Chien, K. D. Closser, D. L. Crittenden, M. Diedenhofen, R. A. DiStasio, H. Do, A. D. Dutoi, R. G. Edgar, S. Fatehi, L. Fusti-Molnar, A. Ghysels, A. Golubeva-Zadorozhnaya, J. Gomes, M. W. D. Hanson-Heine, P. H. P. Harbach, A. W. Hauser, E. G. Hohenstein, Z. C. Holden, T.-C. Jagau, H. Ji, B. Kaduk, K. Khistyaeve, J. Kim, J. Kim, R. A. King, P. Klunzinger, D. Kosenkov, T. Kowalczyk, C. M. Krauter, K. U. Lao, A. D. Laurent, K. V. Lawler, S. V. Levchenko, C. Y. Lin, F. Liu, E. Livshits, R. C. Lochan, A. Luenser, P. Manohar, S. F. Manzer, S.-P. Mao, N. Mardirossian, A. V. Marenich, S. A. Maurer, N. J. Mayhall, E. Neuscamman, C. M. Oana, R. Olivares-Amaya, D. P. O'Neill, J. A. Parkhill, T. M. Perrine, R. Peverati, A. Prociuk, D. R. Rehn, E. Rosta, N. J. Russ, S. M. Sharada, S. Sharma, D. W. Small, A. Sodt, T. Stein, D. Stück, Y.-C. Su, A. J. W. Thom, T. Tsuchimochi, V. Vanovschi, L. Vogt, O. Vydrov, T. Wang, M. A. Watson, J. Wenzel, A. White, C. F. Williams, J. Yang, S. Yeganeh, S. R. Yost, Z.-Q. You, I. Y. Zhang, X. Zhang, Y. Zhao, B. R. Brooks, G. K. L. Chan, D. M. Chipman, C. J. Cramer, W. A. Goddard, M. S. Gordon, W. J. Hehre, A. Klamt, H. F. Schaefer, M. W. Schmidt, C. D. Sherrill, D. G. Truhlar, A. Warshel, X. Xu, A. Aspuru-Guzik, R. Baer, A. T. Bell, N. A. Besley, J.-D. Chai, A. Dreuw, B. D. Dunietz, T. R. Furlani, S. R. Gwaltney, C.-P. Hsu, Y. Jung, J. Kong, D. S. Lambrecht, W. Liang, C. Ochsenfeld, V. A. Rassolov, L. V. Slipchenko, J. E. Subotnik, T. Van Voorhis, J. M. Herbert, A. I. Krylov, P. M. W. Gill and M. Head-Gordon, *Molecular Physics*, 2015, **113**, 184-215.
2. R. Papadakis, H. Li, J. Bergman, A. Lundstedt, K. Jorner, R. Ayub, S. Haldar, B. O. Jahn, A. Denisova, B. Zietz, R. Lindh, B. Sanyal, H. Grennberg, K. Leifer and H. Ottosson, *Nat. Commun.*, 2016, **7**, 12962.
3. D. Kim, *J. Phys. Chem. C*, 2015, **119**, 12690-12697.
4. M. J. Frisch, G. W. Trucks, H. B. Schlegel, G. E. Scuseria, M. A. Robb, J. R. Cheeseman, G. Scalmani, V. Barone, G. A. Petersson, H. Nakatsuji, X. Li, M. Caricato, A. V. Marenich, J. Bloino, B. G. Janesko, R. Gomperts, B. Mennucci, H. P. Hratchian, J. V. Ortiz, A. F. Izmaylov, J. L. Sonnenberg, Williams, F. Ding, F. Lipparini, F. Egidi, J. Goings, B. Peng, A. Petrone, T. Henderson, D. Ranasinghe, V. G. Zakrzewski, J. Gao, N. Rega, G. Zheng, W. Liang, M. Hada, M. Ehara, K. Toyota, R. Fukuda, J. Hasegawa, M. Ishida, T. Nakajima, Y. Honda, O. Kitao, H. Nakai, T. Vreven, K. Throssell, J. A. Montgomery Jr., J. E. Peralta, F. Ogliaro, M. J. Bearpark, J. J. Heyd, E. N. Brothers, K. N. Kudin, V. N. Staroverov, T. A. Keith, R. Kobayashi, J. Normand, K. Raghavachari, A. P. Rendell, J. C. Burant, S. S. Iyengar, J. Tomasi, M. Cossi, J. M. Millam, M. Klene, C. Adamo, R. Cammi, J. W. Ochterski, R. L. Martin, K. Morokuma, O. Farkas, J. B. Foresman and D. J. Fox, *Journal*, 2016.
5. A. Stanger, *J. Org. Chem.*, 2006, **71**, 883-893.
6. Gaussian09, M. J. Frisch, G. W. T.; H. B. Schlegel, G. E. Scuseria, M. A. Robb, J. R. Cheeseman, G. S.; V. Barone, B. Mennucci, G. A. Petersson, H. Nakatsuji, M. Caricato, X. L.; H. P. Hratchian, A. F. Izmaylov, J. Bloino, G. Zheng, J. L. Sonnenberg, M.; Hada, M. Ehara, K. Toyota, R. Fukuda, J. Hasegawa, M. Ishida, T. N.; Y. Honda, O. Kitao, H. Nakai, T. Vreven, J. A. Montgomery, Jr., J. E.; Peralta, F. Ogliaro, M. Bearpark, J. J. Heyd, E. Brothers, K. N. Kudin, V. N.; Staroverov, R. Kobayashi, J. Normand, K. Raghavachari, A. Rendell, J. C.; Burant, S. S. Iyengar, J. Tomasi, M. Cossi, N. Rega, J. M. Millam, M. Klene, J. E. Knox, J. B. Cross, V. Bakken, C. Adamo, J. Jaramillo, R. G.; R. E. Stratmann, O. Yazyev, A. J. Austin, R. Cammi, C. Pomelli, J. W. O.; et al. Gaussian, Inc., Wallingford CT. 2009.

7. A. Rahalkar, A. Stanger, "Aroma". This software may be downloaded free of charge from [http://schulich.technion.ac.il/Amnon\\_Stanger.htm](http://schulich.technion.ac.il/Amnon_Stanger.htm)
8. J. Jusélius, D. Sundholm and J. Gauss, *J. Chem. Phys.*, 2004, **121**, 3952-3963.
9. S. Taubert, D. Sundholm and J. Jusélius, *J. Chem. Phys.*, 2011, **134**, 054123.
10. H. Fliegl, S. Taubert, O. Lehtonen and D. Sundholm, *Phys. Chem. Chem. Phys.*, 2011, **13**, 20500-20518.
11. A. Henderson, ParaView Guide, A Parallel Visualization Application, Kitware Inc., 2007.
12. A. D. Becke and K. E. Edgecombe, *J. Chem. Phys.*, 1990, **92**, 5397-5403.
13. T. Lu and F. Chen, *J. Comp. Chem.*, 2012, **33**, 580-592.
14. D. Chen, T. Shen, K. An and J. Zhu, *Comm. Chem.*, 2018, **1**, 18.
15. T. M. Krygowski, H. Szatylowicz, O. A. Stasyuk, J. Dominikowska and M. Palusiak, *Chem. Rev.*, 2014, **114**, 6383-6422.